Heliyon 10 (2024) e26432

Contents lists available at ScienceDirect

Heliyon

journal homepage: www.cell.com/heliyon

Research article

Entropy generation for exact irreversibility analysis in the MHD channel flow of Williamson fluid with combined convective-radiative boundary conditions☆

Sohail Nadeem [a,b,c,1,*], Bushra Ishtiaq [a], Jehad Alzabut [b,d,1], Hassan Ali Ghazwani [e,**]

[a] Department of Mathematics, Quaid-I-Azam University, 45320, Islamabad 44000, Pakistan
[b] Department of Mathematics and Sciences, Prince Sultan University, 11586, Riyadh, Saudi Arabia
[c] Department of Mathematics, Wenzhou University, Wenzhou, 325035, China
[d] Department of Industrial Engineering, OSTIM Technical University, Ankara 06374, Turkey
[e] Department of Mechanical Engineering, Faculty of Engineering, Jazan University, P.O. Box 45124, Jazan, Saudi Arabia

ARTICLE INFO

Keywords:
Entropy optimization
MHD channel flow
Convective-radiative boundary conditions
Williamson fluid
Viscous dissipation
Joule heating

ABSTRACT

The scrutinization of entropy optimization in the various flow mechanisms of non-Newtonian fluids with heat transfer has been incredibly enhanced. Through the investigation of irreversibility sources in the steady flow of a non-Newtonian Willaimson fluid, an analysis of entropy generation is carried out in this current work. The current study has an essential aspect of investigating the heat transfer mechanism with flow phenomenon by considering convective-radiative boundary conditions. A horizontal MHD channel is assumed with two parallel plates to develop a mathematical model for the flow phenomenon by considering the variable viscosity of the fluid. The contribution of physical impacts of thermal radiation, Joule heating, and viscous dissipation is interpolated in the constitutive energy equation. The complete flow of the current analysis is established in the form of ordinary differential equations which further take the form of the dimensionless system through the contribution of the similarity variables. A graphical scrutinization of the physical features of the flow phenomenon in relation to the pertinent parameters is proposed. This study reveals that the higher magnitude of radiation parameter and Brinkman number dominates the system's entropy. Moreover, the temperature distribution experiences an increasing mechanism with improved conduction-radiation parameter at the lower plate.

1. Introduction

Non-Newtonian fluids have realistic executions in many branches such as biological fluids, rubber industry, drilling operations,

☆ Authors are thankful to PSU for the support.
* Corresponding author at: Department of Mathematics Quaid Azam University Islamabad, Pakistan.
** Corresponding author at: Department of Mechanical Engineering, Faculty of Engineering, Jazan University, P.O. Box 45124, Jazan, Saudi Arabia.
E-mail addresses: snqau@hotmail.com (S. Nadeem), hghazwani@jazanu.edu.sa (H.A. Ghazwani).
[1] Authors are thankful to PSU for the support.

https://doi.org/10.1016/j.heliyon.2024.e26432
Received 26 June 2023; Received in revised form 12 February 2024; Accepted 13 February 2024
Available online 19 February 2024

lubricants, paints, and polymer manufacturing. Navier-Stokes equations do not fulfill the requirement to deliberate the rheological attributes of non-Newtonian fluids. For this purpose, various fluid models have been introduced. Williamson fluid belongs to the non-Newtonian fluid models which have a complicated mathematical model and cannot be detailed via an individual constitutive equation. The pseudoplastic fluid's rheological nature can be explained by developing the model of Williamson fluid. Williamson [1] devoted his consideration to contemplating the concept of the Willaimson fluid model by examining the flow mechanism of pseudoplastic fluid. The nature of the Williamson fluid under unsteady flow conditions on a stretchable medium was disclosed by Shamshuddin et al. [2]. The Williamson fluid with its physical properties and time-independent flow nature subject to different mediums was inspected by Rehman et al. [3]. They discerned that in context to both mediums, the improved fluid parameter minimized the surface drag force. Ahmed et al. [4] conducted a flow analysis on a non-linear stretched medium in a Williamson fluid influenced by a two-phase model. Kada et al. [5] scrutinized the radiative time-independent flow phenomenon with physical conditions in a Willaimson fluid. They deduce that the temperature distribution of the Williamson fluid increases as a result of the greater magnitude of radiation.

In the production of thermal devices in industries, the main concern is the effectual execution of energy. By lowering the entropy generation during the procedure, this goal can be accomplished. There are various factors that participate in the minimization of entropy production namely friction, viscosity loss, heat transfer, etc. Firstly, Bejan [6] improves the effectiveness of the thermal system by reducing entropy generation. Das et al. [7] conducted an examination of entropy optimization in a nanofluid about boundary layer incompressible flow. An examination of the hydromagnetic flow mechanism with physical effects and entropy generation in a Casson nanofluid was also addressed by Das et al. [8]. They observed that entropy optimization experiences a deterioration with the improved Hall current. Ishtiaq et al. [9] ascertain the entropy generation in the flow mechanism of a micropolar nanofluid under the influence of several physical conditions. The magnetized flow mechanism produced within a movable medium in a nanofluid was addressed by Sarfraz and Khan [10] to estimate the entropy process. Hassan et al. [11] examined the factors that contribute to the irreversibility analysis of the flow phenomenon in Eyring-Powell fluid subject to a stretched medium. They noticed an exaggeration in entropy production with the improved exponent parameter.

Various researchers have worked on hydromagnetic flows due to their many implementations in engineering and industries. Examples of such flows include nuclear reactor cooling, Teltron tubes, jet printers, Helmholtz coils, pumps, MHD generators, accelerators, etc. There is numerous work on fluid flows with magnetic effects. The physical characteristics of a magnetized nanofluid under the assumption of vertically oriented parallel plates were revealed by Das et al. [12]. They indicated the degradation of the velocity distribution in relation to the high level of magnetic field. Ahmad et al. [13] showed how to estimate the magnetic effect on a Sisko fluid's steady flow process. On a stretchable biaxial sheet, Sarfraz and Khan [14] inspect the flowing nature of a magnetized nanofluid in context to a stagnant point. Yasir et al. [15] conducted an unsteady study on a stretched medium to scrutinize the physical attributes of the magnetized hybrid nanofluid. They explored the dual behavior of the outcomes. Usman et al. [16] revealed the non-similar outcomes of the magnetized flow mechanisms generated by distinct configurations in a nanofluid. The significance of the magnetic field on the flow properties of a Newtonian fluid with its thermal characteristics was scrutinized by Usman et al. [17]. They deduce that the improved magnetic field declines mass diffusion. Asmat et al. [18] demonstrated the magnetized flow phenomenon developed in one dimension by an oscillatory medium in a viscous fluid with nanoparticles. Similarly, many problems of magnetohydrodynamics flows have been introduced in Refs. [19–25].

To estimate the radiative heat flux, numerous researchers executed a mathematical linear model to scrutinize the heat transport mechanisms of different fluids with physical conditions. Das et al. [26] analyzed the effect of thermal radiation on the mechanism of heat transfer in a Casson nanofluid subject to a horizontal medium. With the assumption of two rotating plates, the radiative flow with viscous dissipation impact in a Casson fluid comprising nanoparticles was also inspected by Das et al. [27]. Musa et al. [28] carried out an evaluation of the flow behavior of a nanofluid with the significance of thermal radiation. Through a channel, the physical consequences of convective heating and thermal radiation on the flow of an incompressible nanofluid were demonstrated by Yu and Wang [29]. With the contribution of radiative impacts, the heat transport mechanism in a Newtonian fluid relative to a smooth medium was deliberated by Asmat et al. [30].

In the current analysis, a non-Newtonian model of Willaimson fluid is considered with its variable characteristics to explore the entropy optimization in the magnetized flow mechanism within a channel having parallel horizontal plates. The current study is novel as no one explores the entropy optimization and heat transfer mechanism of Williamson fluid in a channel corresponding to the convective-radiative boundary conditions. The convective-radiative boundary conditions with the collaboration of thermal radiation, viscous dissipation, and joule heating participate in the scrutinization of the heat transport phenomenon. Various irreversible factors are indicated to demonstrate the process of entropy generation. A graphical illustration is prepared to observe the consequences of emerging parameters on the temperature, entropy generation, and velocity profiles.

2. Description of the flow problem

To examine the flow behavior of Willaimson fluid subject to the variable temperature-dependent viscosity, we take a horizontal channel with two parallel plates. The two considered plates departed with each other with distance a. The steady flow mechanism is observed by considering a constant magnetic field which is practiced in the $\widetilde{y}$ direction transversely. The lower plate is situated at $\widetilde{y} = 0$ while the upper plate takes the position at $\widetilde{y} = a$, the transversal coordinate. For the ongoing analysis, the flow field has only one component of velocity dependent on the $\widetilde{y}$ coordinate in the axial direction due to the infinitely long plates. The upper plate has a connection with the ambient fluid T_a while the considered hot fluid conveys the temperature T_h to the lower plate by convection. Moreover, the energy equation is composed of taking into account the influences of Joule heating, thermal radiation, and viscous

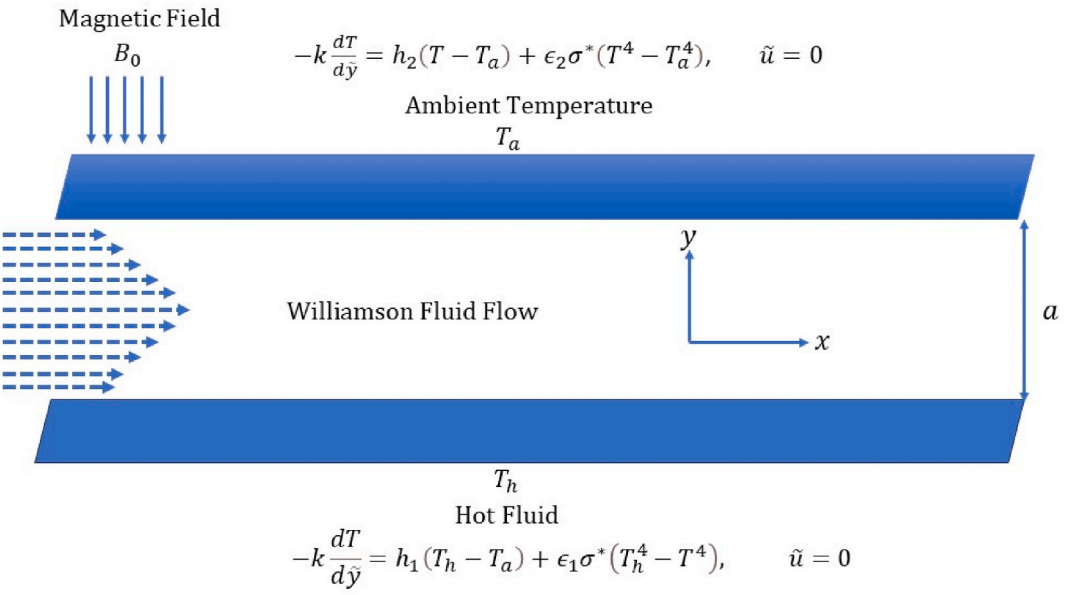

Fig. 1. Physical configuration of problem.

dissipation. To analyze the heat transport mechanism, the convective-radiative physical boundary conditions are implemented. The complete geometrical explanation is disclosed in Fig. 1.

For the concerned Williamson fluid, the relevant constitutive equations are depicted in Eqs. (1) and (2) as follows [31].

$$\boldsymbol{S} = -p\boldsymbol{I} + \boldsymbol{\tau}, \tag{1}$$

$$\boldsymbol{\tau} = \left[\mu_\infty + (1 - \Gamma\gamma)^{-1}(\mu_0 - \mu_\infty)\right]\boldsymbol{A}, \tag{2}$$

Here we consider the case of $\Gamma\gamma < 1$ and $\mu_\infty = 0$. Eq. (2) converts into Eq. (3) as follows

$$\boldsymbol{\tau} = \left[(1 - \Gamma\gamma)^{-1}\mu_0\right]\boldsymbol{A}, \tag{3}$$

After executing the binomial expansion, Eq. (3) transform into Eq. (4) as follows

$$\boldsymbol{\tau} = \mu_0[1 + \Gamma\gamma]\boldsymbol{A}, \tag{4}$$

In Eq. (4), the expression of γ is define in Eq. (5) as follow [31]

$$\gamma = \sqrt{(1/2)\pi}, \pi = tr(\boldsymbol{A}^2), \tag{5}$$

Eq. (5) can be written in the form as given in Eq. (6)

$$\gamma = {}^{1}\Big/\left(2(\widetilde{v}_{\tilde{y}})^2 + (\widetilde{v}_{\tilde{x}} + \widetilde{u}_{\tilde{y}})^2 + 2(\widetilde{u}_{\tilde{x}})^2\right)^{-0.5}, \tag{6}$$

The desired components of the tensor are acquired after utilizing Eqs. (4) and (6). These components are defined in Eq. (7) as follows

$$\begin{aligned}
\tau_{xx} &= 2(\widetilde{u}_{\tilde{x}})\mu_0\left[1 + \Gamma\left\{{}^{1}\Big/\left((\widetilde{v}_{\tilde{x}} + \widetilde{u}_{\tilde{y}})^2 + 2(\widetilde{v}_{\tilde{y}})^2 + 2(\widetilde{u}_{\tilde{x}})^2\right)^{-0.5}\right\}\right], \\
\tau_{yx} &= \tau_{xy} = (\widetilde{u}_{\tilde{y}} + \widetilde{v}_{\tilde{x}})\mu_0\left[1 + \Gamma\left\{{}^{1}\Big/\left((\widetilde{v}_{\tilde{x}} + \widetilde{u}_{\tilde{y}})^2 + 2(\widetilde{v}_{\tilde{y}})^2 + 2(\widetilde{u}_{\tilde{x}})^2\right)^{-0.5}\right\}\right] \\
\tau_{yy} &= (\widetilde{v}_{\tilde{y}})2\mu_0\left[1 + \Gamma\left\{{}^{1}\Big/\left((\widetilde{v}_{\tilde{x}} + \widetilde{u}_{\tilde{y}})^2 + 2(\widetilde{v}_{\tilde{y}})^2 + 2(\widetilde{u}_{\tilde{x}})^2\right)^{-0.5}\right\}\right].
\end{aligned} \tag{7}$$

With the help of the above equations and flow assumptions, the constitutive equations have the following expressions which are given in Eqs. (8) and (9) as follows [32].

$$0 = -\frac{dp}{d\tilde{x}} + \frac{d}{d\tilde{y}}\left(\mu(T)\left(\frac{d\tilde{u}}{d\tilde{y}} + \sqrt{2}\,\Gamma\left(\frac{d\tilde{u}}{d\tilde{y}}\right)^2\right)\right) - \sigma B_0^2 \tilde{u}, \tag{8}$$

$$0 = k\frac{d^2T}{d\tilde{y}^2} + \mu(T)\left(1 + \sqrt{2}\,\Gamma\frac{d\tilde{u}}{d\tilde{y}}\right)\left(\frac{d\tilde{u}}{d\tilde{y}}\right)^2 - \frac{dq_r}{d\tilde{y}} + \sigma B_0^2 \tilde{u}^2, \tag{9}$$

In Eqs. (8) and (9), the following expression of variable viscosity and radiative heat flux are executed [32,33], which are given in Eq. (10).

$$\mu(T) = \mu_f e^{-b_1(T-T_a)} = \mu_f(1 - b_1(T - T_a))\; q_r = = -\frac{4\sigma^*}{3k_1}\frac{dT^4}{d\tilde{y}} = -\frac{16\sigma^*}{3k_1}T^3\frac{dT}{d\tilde{y}}, \tag{10}$$

The appropriate boundary conditions are depicted in Eq. (11) as follows [32,33].

$$\text{at}\quad \tilde{y} = 0, \tilde{u} = 0, \text{at}\quad \tilde{y} = a, \tilde{u} = 0, -k\frac{dT}{d\tilde{y}} = h_1(T_h - T_a) + \epsilon_1\sigma^*\left(T_h^4 - T^4\right)\quad \text{at}\quad \tilde{y} = 0, -k\frac{dT}{d\tilde{y}} = h_2(T - T_a) + \epsilon_2\sigma^*\left(T^4 - T_a^4\right)\quad \text{at}\quad \tilde{y} = a.. \tag{11}$$

Now, familiarize the following dimensionless variables [32] which are manifested in Eq. (12).

$$U = \tilde{u}a\rho/\mu_f, Y = \tilde{y}/a, \mu = \mu(T)/\mu_f, \theta = T - T_a/T_h - T_a, \theta_h = T_h/T_a \tag{12}$$

The implementation of Eq. (12) into Eqs. (8) and (9) with (10) yields the following Eqs. (13) and (14).

$$(1 - b_v\theta(Y))\frac{d^2U}{dY^2} - b_v\frac{dU}{dY}\frac{d\theta}{dY} + \delta\left(2(1 - b_v\theta(Y))\frac{dU}{dY}\frac{d^2U}{dY^2} - b_v\frac{d\theta}{dY}\left(\frac{dU}{dY}\right)^2\right) - H_a^2U(Y) + P = 0, \tag{13}$$

$$\frac{d^2\theta}{dY^2} + \frac{Br}{(\theta_h - 1)}(1 - b_v\theta(Y))\left(1 + \delta\frac{dU}{dY}\right)\left(\frac{dU}{dY}\right)^2 + Rd((\theta_h - 1)\theta + 1)^3\frac{d^2\theta}{dY^2} + \frac{H_a^2Br}{(\theta_h - 1)}(U(Y))^2 = 0, \tag{14}$$

Eq. (11) transform into the following Eq. (15) as follows

$$\text{at}\quad Y = 0, U(Y) = 0, \text{at}\quad Y = 1, U(Y) = 0, \frac{d\theta(Y)}{dY} + Bi_0(-\theta(Y) + 1) + \frac{Nr_0}{(\theta_h - 1)}\left(\theta_h^4 - \left((\theta_h - 1)\theta(Y) + 1\right)^4\right) = 0\quad \text{at}\quad Y = 0, \frac{d\theta(Y)}{dY} + Bi_1\theta(Y) + \frac{Nr_1}{(\theta_h - 1)}\left(\left((\theta_h - 1)\theta(Y) + 1\right)^4 - 1\right) = 0\quad \text{at}\quad Y = 1.. \tag{15}$$

The parameters with dimensionless form involved in the afore-mentioned equations are defined in the following Eq. (16).

$$b_v = b_1(T_h - T_a), \delta = \frac{\sqrt{2}\Gamma\mu_f}{a^2\rho}, Ha = aB_0\sqrt{\sigma/\mu_f}, P = -\left(\frac{dp}{d\tilde{x}}\right)\frac{a^3\rho}{\mu_f^2}, Br = \frac{\mu_f^3}{k\rho^2a^2T_a}, Rd = \frac{16\sigma^*T_a^3}{3k_1k}, Bi_0 = \frac{ah_1}{k}, Bi_1 = \frac{ah_2}{k}, Nr_0 = \frac{a\epsilon_1\sigma^*T_a^3}{k}, Nr_1 = \frac{a\epsilon_2\sigma^*T_a^3}{k}.. \tag{16}$$

It is noted that the case of $b_v = 0$ leads to the constant viscosity of the concerned fluid. By taking $b_v = 0$ and $\delta = 0$, we acquire the exact solution to Eq. (13) corresponding to the boundary conditions which is given in Eq. (17).

$$U(Y) = -\frac{e^{-HaY}(e^{HaY} - 1)(e^{HaY} - e^{Ha})P}{(1 + e^{Ha})H_a^2} \tag{17}$$

With the exclusion of thermal radiation and conduction-radiation parameters, Eq. (14) has the following exact solution which is depicted in Eq. (18).

$$\begin{aligned}\theta(Y) = \big[&e^{-2HaY}\big(-2Bi_0e^{2HaY}Ha^4 + 2\theta_hBi_0e^{2HaY}Ha^4 - 2Bi_0Bi_1e^{2HaY}Ha^4 + 2\theta_hBi_0Bi_1e^{2HaY}Ha^4\\ &-4Bi_0e^{Ha+2HaY}Ha^4 + 4\theta_hBi_0e^{Ha+2HaY}Ha^4 - 4Bi_0Bi_1e^{Ha+2HaY}Ha^4 - 2Bi_0e^{2Ha+2HaY}Ha^4\\ &+4\theta_hBi_0Bi_1e^{Ha+2HaY}Ha^4 + 2\theta_hBi_0e^{2Ha+2HaY}Ha^4 - 2Bi_0Bi_1e^{2Ha+2HaY}Ha^4 - Bi_0Bre^{2Ha}P^2\\ &+2\theta_hBi_0Bi_1e^{2Ha+2HaY}Ha^4 - Bi_0Bi_1Bre^{2Ha}P^2 - 3Bi_0Bre^{2HaY}P^2 - 3Bi_1Bre^{2HaY}P^2\\ &-Bi_1Bre^{2Ha}P^2 - Bi_0Bre^{4HaY}P^2 - 3Bi_0Bi_1Bre^{2HaY}P^2 + 4Bi_0Bre^{3HaY}P^2 + 4Bi_1Bre^{3HaY}P^2\\ &+4Bi_0Bi_1Bre^{3HaY}P^2 - Bi_1Bre^{4HaY}P^2 - Bi_0Bi_1Bre^{4HaY}P^2 + 4Bi_0Bre^{Ha+HaY}P^2\end{aligned}$$

$$+4Bi_1Bre^{Ha+HaY}P^2+4Bi_0Bi_1Bre^{Ha+HaY}P^2+4Bi_0Bre^{2Ha+HaY}P^2+4Bi_1Bre^{2Ha+HaY}P^2$$

$$+4Bi_0Bi_1Bre^{2Ha+HaY}P^2-8Bi_0Bre^{Ha+2HaY}P^2-8Bi_1Bre^{Ha+2HaY}P^2+4Bre^{2HaY}HaP^2$$

$$-8Bi_0Bi_1Bre^{Ha+2HaY}P^2-3Bi_0Bre^{2Ha+2HaY}P^2-3Bi_1Bre^{2Ha+2HaY}P^2+2Bre^{2HaY}Ha^2P^2$$

$$-3Bi_0Bi_1Bre^{2Ha+2HaY}P^2+4Bi_0Bre^{Ha+3HaY}P^2+4Bi_1Bre^{Ha+3HaY}P^2+2BrBi_1e^{2HaY}HaP^2$$

$$+4Bi_0Bi_1Bre^{Ha+3HaY}P^2-4Bre^{2Ha+2HaY}HaP^2-2BrBi_1e^{2Ha+2HaY}HaP^2+2Bre^{2HaY}Ha^2P^2$$

$$+BrBi_1e^{2HaY}Ha^2P^2+4Bre^{Ha+2HaY}Ha^2P^2+2BrBi_1e^{Ha+2HaY}Ha^2P^2+2Bre^{2Ha+2HaY}Ha^2P^2$$

$$+BrBi_1e^{2Ha+2HaY}Ha^2P^2+2Bi_0Bi_1e^{2HaY}Ha^4Y-2BrBi_1e^{2HaY}HaP^2Y$$

$$+4Bi_0Bi_1e^{Ha+2HaY}Ha^4Y-4\theta_hBi_0Bi_1e^{Ha+2HaY}Ha^4Y-BrBi_0e^{2HaY}Ha^2P^2Y$$

$$+2Bi_0Bi_1e^{2Ha+2HaY}Ha^4Y-2\theta_hBi_0Bi_1e^{2Ha+2HaY}Ha^4Y-2Bi_0Bre^{2Ha+2HaY}HaP^2Y$$

$$-2\theta_hBi_0Bi_1e^{2HaY}Ha^4Y+2BrBi_1e^{2Ha+2HaY}HaP^2Y+2Bi_0Bre^{2HaY}Ha^2P^2Y$$

$$+Bi_0Bi_1Bre^{2HaY}Ha^2P^2Y+4BrBi_0e^{Ha+2HaY}Ha^2P^2Y+2Bi_0Bi_1Bre^{Ha+2HaY}Ha^2P^2Y$$

$$+\left(2BrBi_0+Bi_0Bi_1Br\right)e^{2Ha+2HaY}Ha^2P^2Y-(2Bi_1Br+BrBi_0Bi_1)e^{2HaY}Ha^2P^2Y$$

$$-(2Bi_0Br+2BrBi_1+2Bi_0Bi_1Br)e^{Ha+2HaY}Ha^2P^2Y-BrBi_0e^{2Ha+2HaY}Ha^2P^2Y$$

$$-Bi_1Bre^{2Ha+2HaY}Ha^2P^2Y-Bi_0Bi_1Bre^{2Ha+2HaY}Ha^2P^2Y+2Bi_0Bre^{2HaY}HaP^2Y)\Big]\Big/$$

$$\left[2(-1+A)(Bi_0+Bi_1+Bi_0Bi_1)\left(1+e^{Ha}\right)^2Ha^4\right] \tag{18}$$

For the ongoing problem, the expressions of engineering interesting quantities of Nusselt number and skin friction coefficient are elucidated in Eq. (19) as follows

$$C_f=\rho a^2\tau_w\Big/\mu_f^2,\ \tau_w=\tau_{xy}=\mu(T)\left(1+\sqrt{2}\,\Gamma\frac{d\widetilde{u}}{d\widetilde{y}}\right)\frac{d\widetilde{u}}{d\widetilde{y}}\bigg|_{\widetilde{y}=0,a}\quad Nu=aq_w\Big/k(T_h-T_a),\ q_w=-\left(k+\frac{16\sigma^*}{3k_1}T^3\right)\frac{dT}{d\widetilde{y}}\bigg|_{\widetilde{y}=0,a} \tag{19}$$

The dimensionless expression of Eq. (19) is defined in Eq. (20) as follows

$$C_f=(1-b_v\theta(Y))\left(1+\delta\frac{dU}{dY}\right)\frac{dU}{dY}\bigg|_{Y=0,1}\quad Nu=-\left(1+Rd((\theta_h-1)\theta(Y)+1)^3\right)\frac{d\theta}{dY}\bigg|_{Y=0,1} \tag{20}$$

3. Assessment of entropy generation

There are various irreversibility processes that become the reason for the development of entropy in the thermal system. This production of entropy affects the energy of the thermal system. So, it is necessary to evaluate the entropy optimization rate by analyzing the irreversibility factors. For the ongoing analysis, the factors that participate in the development of entropy are heat transfer, viscous dissipation, and Joule heating. In terms of these sources, the entropy generation has the following form of the local volumetric rate [34,35] which is manifested in Eq. (21).

$$S_G=\left(k/T^2\right)\left(1+\frac{16\sigma^*T^3}{3k_1k}\right)\left(\frac{dT}{d\widetilde{y}}\right)^2+\left(\mu(T)/T\right)\left(1+\frac{1}{\sqrt{2}}\Gamma\frac{d\widetilde{u}}{d\widetilde{y}}\right)\left(\frac{d\widetilde{u}}{d\widetilde{y}}\right)^2+\frac{\sigma B_0^2\widetilde{u}^2}{T}, \tag{21}$$

In dimensionless form, the entropy estimation has the following expression, defined in Eq. (22).

$$N_G=\frac{(\theta_h-1)^2}{((\theta_h-1)\theta(Y)+1)^2}\left(1+Rd((\theta_h-1)\theta(Y)+1)^3\right)\left(\frac{d\theta}{dY}\right)^2+\frac{Br}{(\theta_h-1)\theta(Y)+1}(1-b_v\theta(Y))\left(1+\delta\frac{dU}{dY}\right)\left(\frac{dU}{dY}\right)^2$$
$$+\frac{H_a^2Br}{(\theta_h-1)\theta(Y)+1}(U(Y))^2. \tag{22}$$

In Eq. (21), N_G is normalized by $\frac{k}{a^2}$.

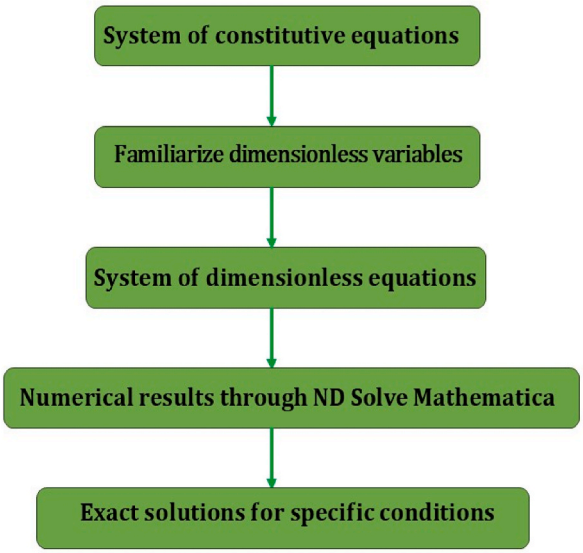

Fig. 2. Problem's flow chart.

Table 1
Comparative values of skin friction coefficient for $Ha = 0.8$ and $Rd = 0.5$.

	Skin friction coefficient	
Y	Present Outcomes	Abbas et al. [36]
0.0	0.87543	0.88869
0.05	0.09419	0.09502
0.1	0.09775	0.09859

Table 2
Comparison of numerical and exact outcomes of velocity and temperature fields when $Ha = 0.5, \theta_h = 2.0, P = Br = Bi_0 = Bi_1 = 1$..

Y	Numerical outcomes $U[Y]$	Exact outcomes $U[Y]$	Numerical outcomes $\theta[Y]$	Exact outcomes $\theta[Y]$
0.1	0.044003	0.044003	0.677003	0.677003
0.2	0.078114	0.078114	0.645143	0.645143
0.3	0.102418	0.102418	0.612398	0.612398
0.4	0.116976	0.116976	0.579235	0.579235
0.5	0.121825	0.121825	0.545928	0.545928

4. Explanations of the results

An analysis of entropy generation in the steady flow mechanism of Williamson fluid under the influence of convective-radiative physical conditions and various physical effects is the main concern of this study. The graphical outcomes of the flow phenomenon are tackled in this section. With the help of the symbolic package Mathematica, different characteristics including heat transfer rate, flow velocity, entropy generation, temperature field, and surface drag force are briefly explicated through tables and graphs. The physical visualization of the current study through a flow chart is illustrated in Fig. 2. For the confirmation and accuracy of the ongoing problem, the skin friction coefficient with its numerical values is demonstrated in Table 1 for distinct pertinent parameters and compared with the previous study. A satisfactory correspondence is exhibited between the current findings and earlier results which confirm the validity of the ongoing problem. Moreover, the numerical and exact outcomes are compared in Table 2 for both temperature and velocity fields. Comparative values in Table 2 show that an excellent relationship exists in both numerical and exact solutions. The pertinent parameters exhibit notable influences on the flow characteristics which are revealed in Figs. 3–13. The profile of the temperature distribution in relation to the radiation and Brinkman parameters is manifested in Figs. 3 and 4 respectively. From these curves, it is ascertained that both the parameters with their greater intensity improve the temperature distribution. The reason behind this phenomenon is that more heat is conveyed to the concerned fluid with the higher magnitude of the radiation parameter which ameliorates the thickness of the thermal boundary layer. The correspondence between the transfer of heat by molecular conduction and heat developed by viscous dissipation is manifested by the Brinkman number. Thus, the process of heat conduction becomes lower with the larger amount of the Brinkman number and an increment is developed in the viscous heating of the fluid.

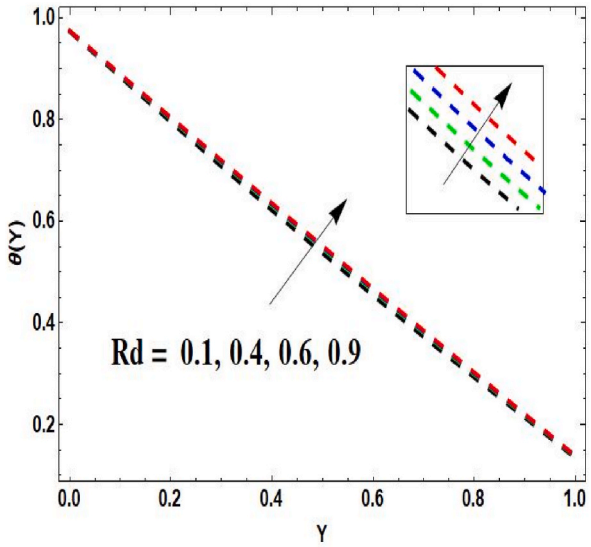

Fig. 3. Radiation parameter related temperature field.

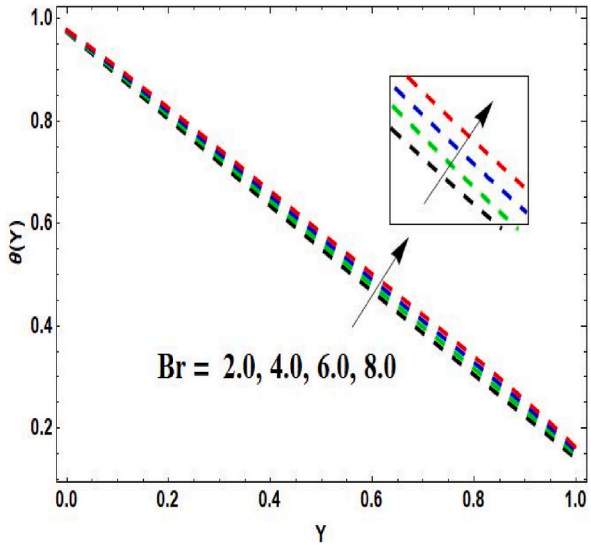

Fig. 4. Brinkman number related temperature field.

Accordingly, the temperature inside the channel is intensified. The significance of the greater magnitude of both lower and upper plates Biot numbers on the profile of the fluid temperature is disclosed in Figs. 5 and 6 respectively. These graphics exhibit that the temperature distribution dominates with the lower plate Biot number but exhibits deteriorating behavior with the upper plate Biot number. Physically, the transport of heat at the lower plate through convection improves the thermal boundary layer's thickness. As a consequence, the temperature rises with the presence of the greater magnitude of the lower plate Biot number. The influence of the conduction-radiation parameter relative to the lower and upper plates on the temperature curve is the same as of Biot numbers, manifested in Figs. 7 and 8 respectively. This mechanism is held with the fact that the movement of heat from the upper plate to the surroundings is enhanced with the improved conduction-radiation parameter. Due to this, the temperature at the upper plate becomes lower. As a result of the greater amount of the parameter, however, the heat transfer rate inclines at the lower plate. Consequently, the temperature exhibits an exaggerated nature at the lower part of the channel. The graphical nature of the flow velocity against the improved variable viscosity parameter is revealed in Fig. 9. The graphics of the velocity field indicate that the improved variable viscosity parameter strengthens the curve. This phenomenon is physically true because the temperature difference has a direct relation with the parameter of variable viscosity which lowers the fluid dynamic viscosity. Consequently, the flow velocity demonstrates the rising phenomenon. Fig. 10 is prepared to inspect the behavior of the flow field regarding the Williamson fluid parameter. This illustration revealed that within the flow field at $Y = 0.45$, an inflection point is established. At the channel's lower side, the fluid

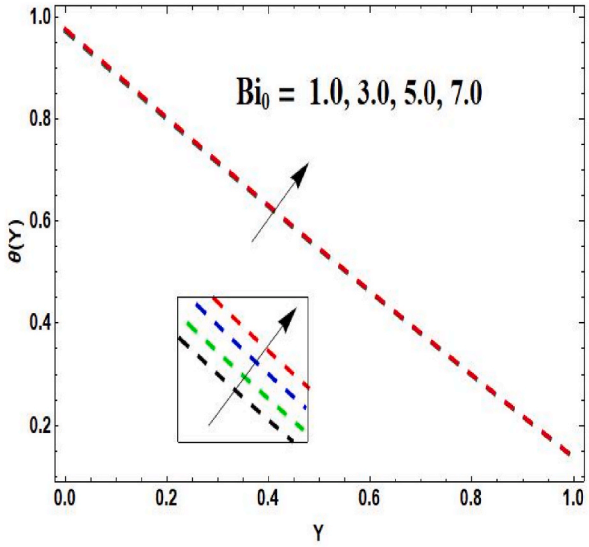

Fig. 5. Lower plate Biot number related temperature field.

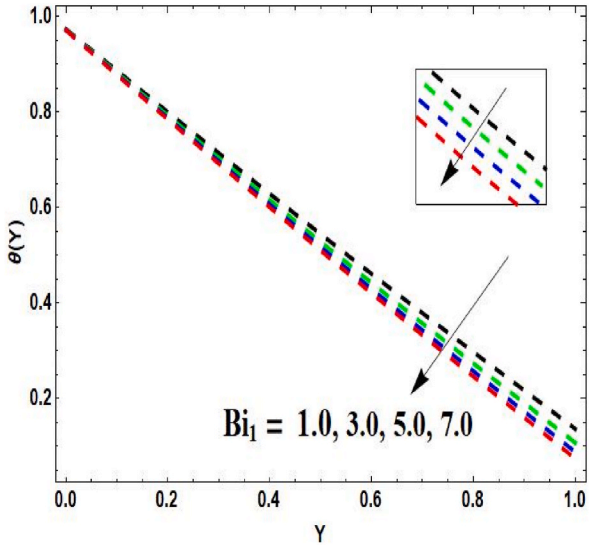

Fig. 6. Upper plate Biot number related temperature field.

velocity shows a reduction, but it exhibits the opposite behavior at the upper plate. Physically, this phenomenon occurs due to the enhanced relaxation time with the improved Williamson fluid parameter. With excessive relaxation time, there is higher resistance to the passage of the relevant fluid inside the channel. As a result, the velocity becomes declines with the strongest resistance. Fig. 11 is prepared to explore the declining nature of the fluid flow in the context of the Hartmann number. The collaboration of the magnetic field and induced electric current develops a resistive Lorentz force. This resistive force diminishes the motion of the fluid in the axial direction. To ascertain the nature of the entropy optimization curve corresponding to the radiation parameter, Brinkman number, and Hartmann number, Figs. 12–14 are prepared. An augmented behavior of entropy generation is observed in Fig. 12 with the escalating values of the radiation parameter. An inverse relationship exists between the radiation and mean absorption parameters. The mean absorption coefficient becomes lessens with the greater radiation parameter. Accordingly, the concerned fluid consumes a slighter amount of energy, and an inclination is developed in the entropy. In Fig. 13, the acceleration in the Brinkman number demonstrates the same effect on entropy generation as that of the radiation parameter. This phenomenon is held due to the reason that heat generation is presented by the Brinkman number. Thus, the improving Brinkman number develops additional heat in the fluid's layers. Consequently, the entropy generation rate escalated inside the channel. The interesting fact in this graphic is that the entropy production exhibits accelerating behavior at the lower and upper sides of the channel, but it is not affected by the Brinkman number at the center of the channel in the range of $0.4 \leq Y \leq 0.6$. Fig. 14 elucidates the significance of the Hartmann number on entropy optimization. With

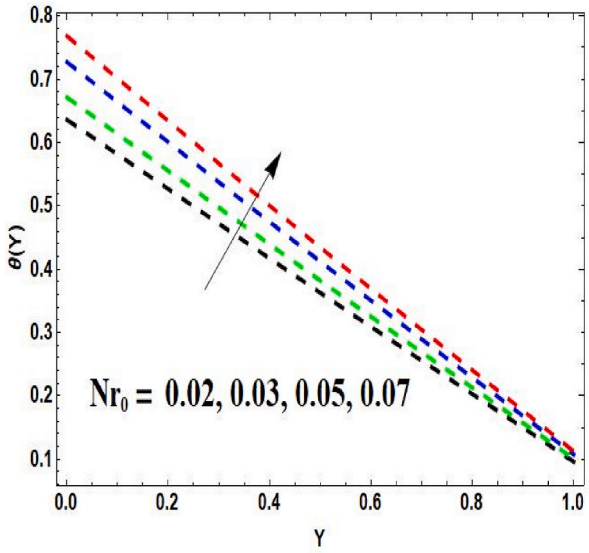

Fig. 7. Lower plate conduction-radiation parameter related temperature field.

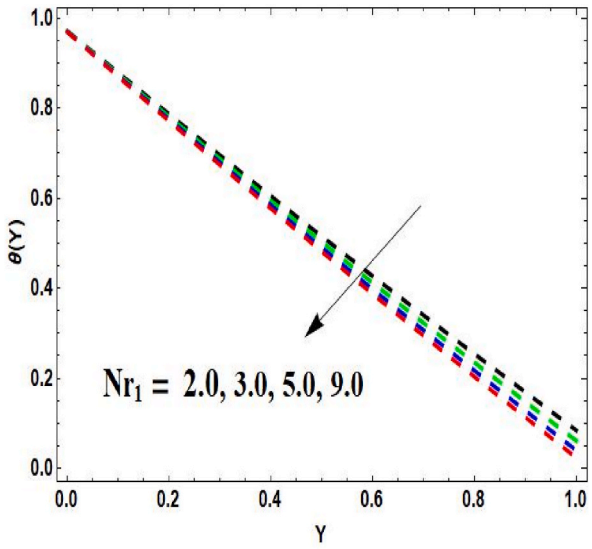

Fig. 8. Upper plate conduction-radiation parameter related temperature field.

the larger magnitude of the Hartmann number, the entropy of the system presents an interesting behavior. It is noticed that at the channel center, the rate of entropy production enhances but it comes to dwindle at the channel's upper and lower plates. Moreover, the two points at $Y = 0.3$ and $Y = 0.7$ exist in the flow field where the system entropy exhibits the negligible impact of the Hartmann number.

The significance of the dimensionless parameters on the physical quantities at both sides of the channel is evaluated through numerical values in Table 3. The heat transfer rate is seen to decrease at the lower plate, whereas, at the upper plate, it is seen to behave differently when the Williamson fluid parameter increases in magnitude. For the same parameter, the surface drag force exhibits an opposite behavior to that of the Nusselt number on both sides of the channel. The higher amount of the Hartmann number exaggerates the rate of heat transport at the lower plate but deteriorates the rate at the upper plate. Meanwhile, the skin friction coefficient becomes declines on both plates for the Hartmann number. On both sides, the local Nusselt number presents an augmented behavior due to the high significance of the lower and upper conduction-radiation parameters. For surface drag force, the higher intensities of these parameters exhibit an accelerating significance at the upper plate but produce a dwindling effect at the lower plate.

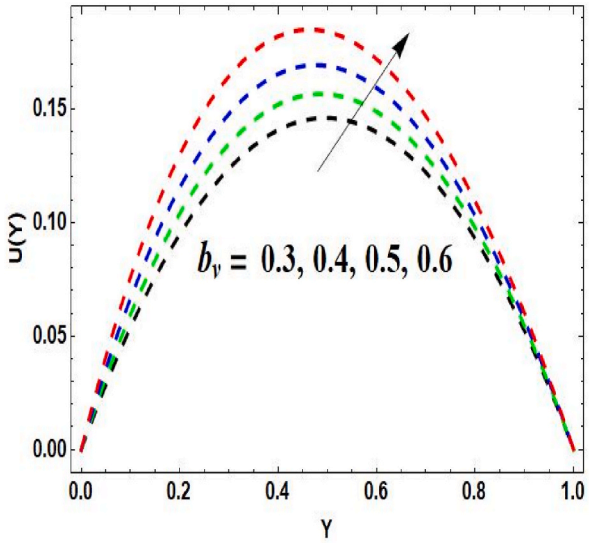

Fig. 9. Variable viscosity parameter related velocity field.

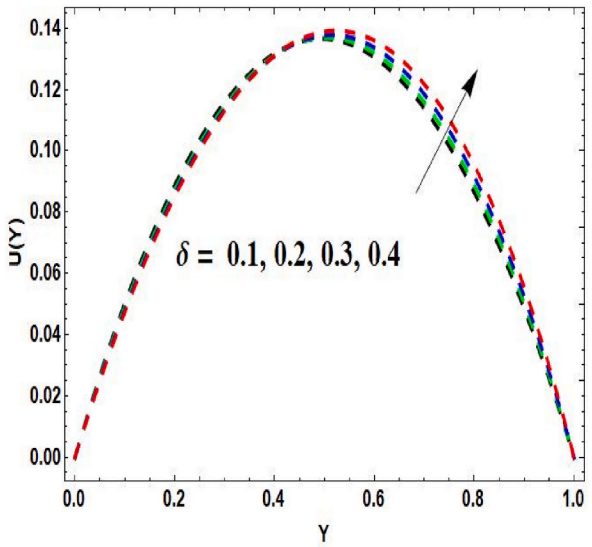

Fig. 10. Williamson fluid parameter related velocity field.

5. Concluding remarks

A brief investigation of the hydromagnetic channel flow phenomenon with entropy optimization in a non-Newtonian Williamson fluid is revealed in this analysis. The heat transform mechanism is scrutinized with distinct physical effects which contribute to the energy equation. The exact result of the fluid velocity is incorporated by considering some specific conditions. Physical significances of several pertinent emerging parameters on the attributes of the flow system are disclosed via graphs and figures. The following points reveal the main observations of the ongoing analysis.

- With the improved conduction-radiation parameter, a large amount of heat is transferred to the surroundings from the upper plate. Resultantly, at the upper plate, the presence of the minimum amount of heat lowers the temperature distribution.
- Due to the existence of an inverse connection between the radiation parameter and the mean absorption parameter, the curve of entropy optimization exposes an inclining nature influenced by the growing magnitude of the radiation parameter.
- The transfer of heat towards the fluid escalated with the increment of the thermal radiation parameter. Consequently, the improved radiation effects escalate the temperature of the fluid.

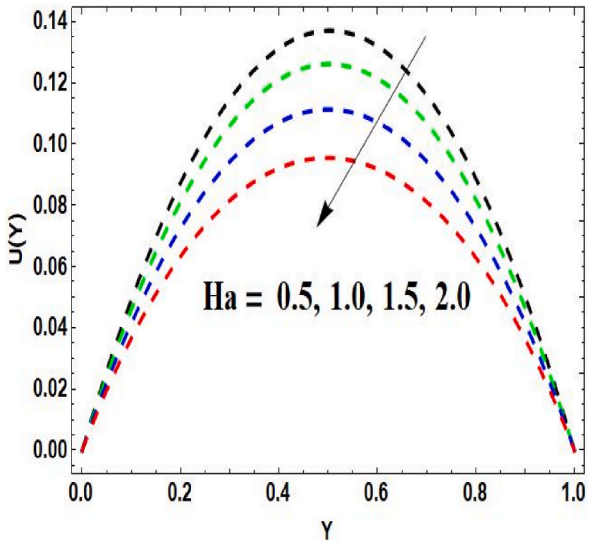

Fig. 11. Hartmann number related velocity field.

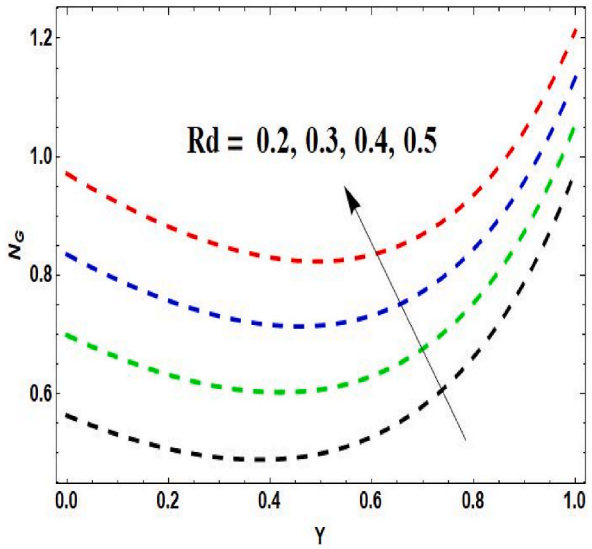

Fig. 12. Radiation parameter related entropy generation.

- With the improved Brinkman number, additional heat is developed within the fluid particles. As a result, the nature of the entropy generation becomes accelerating.
- With the escalating Hartmann number, the development of an opposite Lorentz force within the fluid movement reduces the flow field.
- The existence of the greater values of Williamson fluid generates an opposition in the fluid motion with the higher relaxation time. As a result, the flow distribution declines at the channel's lower side.
- The present study is valid for energy optimization in the magnetized flow of non-Newtonian Williamson fluid with combined convective-radiative conditions. The current problem of entropy optimization can be further explored for various non-Newtonian models by using combined convective-radiative conditions. Moreover, the physical impacts of slip conditions and porosity can also be examined for the present study.

Data availability statement

No data was used for the research described in the article.

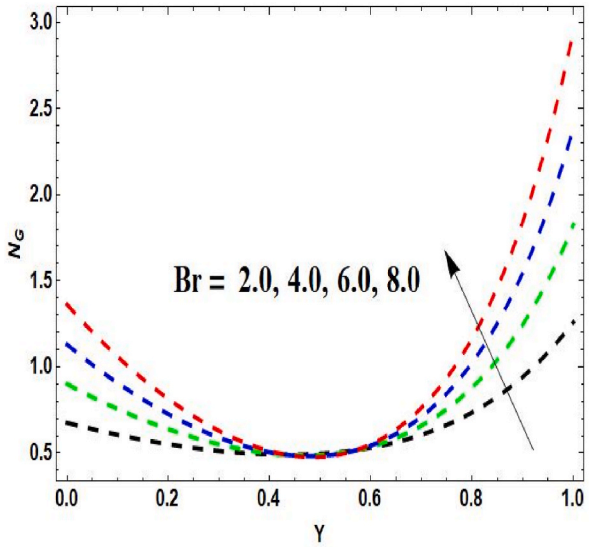

Fig. 13. Brinkman number related entropy generation.

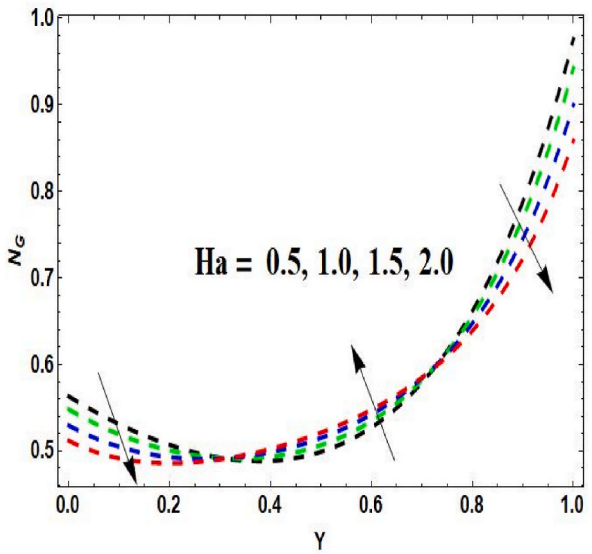

Fig. 14. Hartmann number related entropy generation.

CRediT authorship contribution statement

Sohail Nadeem: Writing – review & editing, Writing – original draft, Supervision, Conceptualization. **Bushra Ishtiaq:** Writing – original draft, Visualization, Software, Formal analysis, Data curation. **Jehad Alzabut:** Visualization, Validation, Resources, Funding acquisition. **Hassan Ali Ghazwani:** Validation, Software, Resources, Project administration, Methodology, Investigation, Data curation.

Declaration of competing interest

The authors declare that they have no known competing financial interests or personal relationships that could have appeared to influence the work reported in this paper.

Table 3
The numerical outcomes of the physical quantities when $b_v = Rd = 0.2, \theta_h = 2.0, P = Br = Bi_0 = Bi_1 = 1$..

				Nu		C_f	
δ	Ha	Nr_0	Nr_1	Upper plate	Lower plate	Upper plate	Lower plate
0.2	0.5	0.2	0.3	0.95697	1.51949	0.48243	0.49449
0.3				0.95718	1.51899	0.47273	0.50401
0.4				0.95763	1.51820	0.46211	0.51432
	1.2			0.95185	1.52572	0.43775	0.44492
	1.4			0.95000	1.52802	0.42124	0.42680
	1.6			0.94808	1.53041	0.40402	0.40801
		0.4		1.00718	1.65762	0.48292	0.49386
		0.5		1.01858	1.68994	0.48303	0.49372
		0.6		1.02647	1.71248	0.48311	0.49362
			0.9	1.01672	1.71979	0.48438	0.49284
			1.2	1.02939	1.76365	0.48481	0.49248
			1.5	1.03819	1.79426	0.48511	0.49223

Acknowledgment

The authors extend their appreciation to the deputyship for research & innovation, Ministry of Education in Saudi Arabia for funding this research work through the project number ISP23-66.

Nomenclature

$(\widetilde{v}, \widetilde{u})$	Velocity elements (m/s)
$\boldsymbol{S}$	Cauchy stress tensor
k	Fluid thermal conductivity $(\mathrm{W(mk)}^{-1})$
δ	Williamson fluid parameter
Γ	Time constant
π	Second invariant strain tensor
σ^*	Stefan-Boltzmann constant $(\mathrm{W/m^2\ K^4})$
P	Pressure gradient parameter
$\boldsymbol{\tau}$	Extra stress tensor
B_0	Magnetic field constant strength $(\mathrm{kg/s^2})$
Nr_0, Nr_1	Conduction-radiation parameters
T	Fluid temperature (K)
k_1	Mean absorption coefficient $\left(\frac{\mathrm{m^2}}{\mathrm{kg}}\right)$
ϵ_1, ϵ_2	Surface emissivities
Br	Brinkman number
p	Fluid pressure (Pa)
μ_∞	Infinite shear rate viscosity (Pa s)
$\boldsymbol{A}$	First Rivlin -Erickson tensor
Ha	Hartmann number
σ	Electrical conductivity $(1/\Omega\mathrm{m})$
q_r	Radiative heat flux (J)
$\boldsymbol{I}$	Identity tensor
Bi_0, Bi_1	Biot numbers
μ_f	Fluid dynamic viscosity (Pa s)
b_1	Viscosity variation parameter
b_v	Variable viscosity parameter
μ_0	Zero shear rate viscosity (Pa s)
h_1, h_2	Convective heat transfer coefficients $\left(\frac{\mathrm{W}}{\mathrm{m^2K}}\right)$
T_a	Ambient temperature (K)
Rd	Radiation parameter

References

[1] R.V. Williamson, The flow of pseudoplastic materials, Ind. Eng. Chem. 21 (11) (1929) 1108–1111.

[2] M.D. Shamshuddin, F. Mabood, S.O. Salawu, Flow of three-dimensional radiative Williamson fluid over an inclined stretching sheet with Hall current and nth-order chemical reaction, Heat Transfer 50 (6) (2021) 5400–5417.
[3] K.U. Rehman, W. Shatanawi, K. Abodayeh, Thermophysical aspects of magnetized Williamson fluid flow subject to both porous and non-porous surfaces: a Lie symmetry analysis, Case Stud. Therm. Eng. 28 (2021) 101688.
[4] K. Ahmed, L.B. McCash, T. Akbar, S. Nadeem, Effective similarity variables for the computations of MHD flow of Williamson nanofluid over a non-linear stretching surface, Processes 10 (6) (2022) 1119.
[5] B. Kada, I. Hussain, A.A. Pasha, W.A. Khan, M. Tabrez, K.A. Juhany, M. Bourchak, R. Othman, Significance of gyrotactic microorganism and bioconvection analysis for radiative Williamson fluid flow with ferromagnetic nanoparticles, Therm. Sci. Eng. Prog. 39 (2023) 101732.
[6] A. Bejan, Second-law analysis in heat transfer and thermal design, Adv. Heat Transfer 15 (1982) 1–58.
[7] S. Das, S. Chakrabort, R.N. Jana, O.D. Makinde, Entropy analysis of nanofluid flow over a convectively heated radially stretching disk embedded in a porous medium, J. Nanofluids 5 (1) (2016) 48–58.
[8] S. Das, S. Sarkar, R.N. Jana, Assessment of irreversible losses of non-Newtonian nanofluid flow underlying Hall current, chemical reaction and thermal radiation, World J. Eng. 18 (2) (2020) 228–250.
[9] B. Ishtiaq, A.M. Zidan, S. Nadeem, M.K. Alaoui, Analysis of entropy generation in the nonlinear thermal radiative micropolar nanofluid flow towards a stagnation point with catalytic effects, Phys. Scripta 97 (8) (2022) 085204.
[10] M. Sarfraz, M. Khan, Entropy generation analysis of CNT-based nanofluid flows induced by a moving plate, Z. Angew. Math. Mech. (2023) 202200555.
[11] M. Hassan, M. Ahsan, Usman, M. Alghamdi, T. Muhammad, Entropy generation and flow characteristics of Powell Eyring fluid under effects of time sale and viscosities parameters, Sci. Rep. 13 (1) (2023) 8376.
[12] S. Das, A.S. Banu, R.N. Jana, O.D. Makinde, Entropy analysis on MHD pseudo-plastic nanofluid flow through a vertical porous channel with convective heating, Alex. Eng. J. 54 (3) (2015) 325–337.
[13] L. Ahmad, J. Ahmed, M. Khan, M. Yasir, M. Alghamdi, Effectiveness of Cattaneo–Christov double diffusion in Sisko fluid flow with variable properties: dual solutions, J. Therm. Anal. Calorim. 143 (5) (2021) 3643–3654.
[14] M. Sarfraz, M. Khan, Significance of Ethylene Glycol-Based CNT Homann Nanofluid Flow over a Biaxially Stretching Surface, Waves in Random and Complex Media, 2022, pp. 1–15.
[15] M. Yasir, A. Hafeez, M. Khan, Thermal conductivity performance in hybrid (SWCNTs-CuO/Ehylene glycol) nanofluid flow: dual solutions, Ain Shams Eng. J. 13 (5) (2022) 101703.
[16] W.A. Usman, N. Uddin Khan, T. Muhammad, Heat and mass transport in an electrically conducting nanofluid flow over two-dimensional geometries, Heliyon 9 (8) (2023) 1.
[17] I. Mustafa Usman, A. Ghaffari, M.S. Iqbal, Unsteady heat and mass transfer in a stagnant flow towards a stretching porous sheet with variable fluid properties, in: Mathematical Modelling of Fluid Dynamics and Nanofluids, 2024, pp. 117–137.
[18] F. Asmat, W.A. Khan, Usman, I. Khan, T. Muhammad, A scientific report on Stokes' second problem for a transient nanofluid model with a heated boundary in the presence of a magnetic field, J. Magn. Magn. Mater. 586 (2023) 171171.
[19] S. Nadeem, M. Tumreen, B. Ishtiaq, N. Abbas, W. Shatanawi, Second-grade nanofluid flow above a vertical slandering Riga surface with double diffusion model, Int. J. Mod. Phys. B 36 (32) (2022) 2250237.
[20] S. Nadeem, B. Ishtiaq, S. Almutairi, H.A. Ghazwani, Impact of Cattaneo–Christov double diffusion on 3d stagnation point axisymmetric flow of second-grade nanofluid towards a riga plate, Int. J. Mod. Phys. B 36 (29) (2022) 2250205.
[21] A.A. Memon, Usman, W.A. Khan, T. Muhammad, Numerical investigation of photovoltaic thermal energy efficiency improvement using the backward step containing Cu-Al2O3 hybrid nanofluid, Alex. Eng. J. 75 (2023) 391–406.
[22] I. Mustafa, S. Shahbaz, Usman, A. Ghaffari, T. Muhammad, Non-similar solution for a power-law fluid flow over a moving wedge, Alex. Eng. J. 75 (2023) 287–296.
[23] M. Alghamdi, A.A. Memon, Usman, T. Muhammad, M.R. Ali, A numerical investigation of a photovoltaic thermal system contained a trapezoidal channel with transport of silver and titanium oxide using the water as base fluids, Case Stud. Therm. Eng. 47 (2023) 103056.
[24] N. Akkurt, T. Shedd, A.A. Memon, Usman, M.R. Ali, M. Bouye, Analysis of the forced convection via the turbulence transport of the hybrid mixture in three-dimensional L-shaped channel, Case Stud. Therm. Eng. 41 (2023) 102558.
[25] S. Nadeem, B. Ishtiaq, N. Abbas, Impact of thermal radiation on two-dimensional unsteady third-grade fluid flow over a permeable stretching Riga plate, Int. J. Mod. Phys. B 37 (1) (2023) 2350009.
[26] S. Das, S. Sarkar, R.N. Jana, Entropy generation analysis of MHD slip flow of non-Newtonian Cu-Casson nanofluid in a porous microchannel filled with saturated porous medium considering thermal radiation, J. Nanofluids 7 (6) (2018) 1217–1232.
[27] S. Das, S. Sarkar, R.N. Jana, Feature of entropy generation in Cu-Al 2 O 3/ethylene glycol hybrid nanofluid flow through a rotating channel, Bionanoscience 10 (2020) 950–967.
[28] A. Musa, A. Hamid, M. Yasir, M. Hussain, Effect of nonlinear thermal radiation and melting heat transfer assessment on magneto-nanofluid through a shrinking surface, waves in random and complex media, 2022, pp. 1–8.
[29] D. Yu, R. Wang, An optimal investigation of convective fluid flow suspended by carbon nanotubes and thermal radiation impact, Mathematics 10 (9) (2022) 1542.
[30] F. Asmat, W.A. Khan, Usman, M.D. Shamshuddin, S.O. Salawu, M. Bouye, Thermal analysis in an electrically conducting fluid with multiple slips and radiation along a plate: a case study of Stokes' second proble, Case Stud. Therm. Eng. 44 (2023) 102831.
[31] U. Shankar, N.B. Naduvinamani, H. Basha, Effect of magnetized variable thermal conductivity on flow and heat transfer characteristics of unsteady Williamson fluid, Nonlinear Eng. 9 (1) (2020) 338–351.
[32] J.C. Umavathi, M.A. Sheremet, S. Mohiuddin, Combined effect of variable viscosity and thermal conductivity on mixed convection flow of a viscous fluid in a vertical channel in the presence of first order chemical reaction, Eur. J. Mech. B Fluid 58 (2016) 98–108.
[33] A. Lopez, G. Ibanez, J. Pantoja, J. Moreira, O. Lastres, Entropy generation analysis of MHD nanofluid flow in a porous vertical microchannel with nonlinear thermal radiation, slip flow and convective-radiative boundary conditions, Int. J. Heat Mass Transfffer 107 (2017) 982–994.
[34] A.A. Opanuga, J.A. Gbadeyan, S.A. Iyase, H.I. Okagbue, Effect of thermal radiation on the entropy generation of hydromagnetic flow through porous channel, Pac. J. Sci. Technol. 17 (2) (2016) 59–68.
[35] N.S. Shashikumar, M. Madhu, S. Sindhu, B.J. Gireesha, N. Kishan, Thermal analysis of MHD Williamson fluid flow through a microchannel, Int. Commun. Heat Mass Transfer 127 (2021) 105582.
[36] Z. Abbas, M. Naveed, M. Hussain, N. Salamat, Analysis of entropy generation for MHD flow of viscous fluid embedded in a vertical porous channel with thermal radiation, Alex. Eng. J. 59 (5) (2020) 3395–3405.